Articles

Kinetics and Thermodynamics of RRF, EF-G, and Thiostrepton Interaction on the *Escherichia coli* Ribosome†

Hyuk-Soo Seo,‡ Michael Kiel,§ Dongli Pan,‡ V. Samuel Raj,§ Akira Kaji,§ and Barry S. Cooperman*,‡

Department of Chemistry, University of Pennsylvania, Philadelphia, Pennsylvania 19104-6323, and Department of Microbiology, School of Medicine, University of Pennsylvania, Philadelphia, Pennsylvania 19104-6076

Received May 25, 2004; Revised Manuscript Received July 17, 2004

ABSTRACT: Ribosome recycling factor (RRF) and elongation factor-G (EF-G) are jointly essential for recycling bacterial ribosomes following termination of protein synthesis. Here we present equilibrium and rapid kinetic measurements permitting formulation of a minimal kinetic scheme that accounts quantitatively for RRF and EF-G interaction on the *Escherichia coli* ribosome. RRF and EF-G (a) each form a binary complex on binding to a bare ribosome which undergoes isomerization to a more stable complex, (b) form mixed ternary complexes on the ribosome in which the affinity for each factor is considerably lower than its affinity for binding to a bare ribosome, and (c) each bind to two sites per ribosome, with EF-G having considerably higher second-site affinity than RRF. Addition of EF-G to the ribosome−RRF complex induces rapid RRF dissociation, at a rate compatible with the rate of ribosome recycling *in vivo*, but added RRF does not increase the lability of ribosome-bound EF-G. Added thiostrepton slows the initial binding of EF-G, and prevents both formation of the more stable EF-G complex and EF-G-induced RRF dissociation. These findings are relevant for the mechanism of post-termination complex disassembly.

Current progress in the structural elucidation of bacterial ribosomes (*1*−*5*) has spurred renewed interest in determining the precise mechanisms by which the ribosome catalyzes protein synthesis (*6*). Disassembly of the post-termination complex, the last step in protein synthesis, is unique in requiring the simultaneous presence of two soluble factors, ribosome recycling factor (RRF)[1] and elongation factor-G (EF-G). The interaction of these two factors on the ribosome has previously been studied by a variety of approaches (*7*−*17*), but the precise mechanism of the disassembly process remains unclear (*9*, *14*, *18*, *19*).

Recently, Kiel *et al*. (*15*) exploited a Millipore filtration technique to investigate RRF−EF-G interactions on the ribosome. They found that in the presence of either GTP, GDPCP (a GTP analogue in which the β- and γ-phosphates are bridged by a CH_2 group), or GDP, added EF-G induces the release of RRF from the ribosome by weakening its affinity. This effect was essentially the same whether it was measured on a bare ribosome or in a model termination complex containing both discharged tRNA and mRNA, and was largely prevented by added thiostrepton. These and other results were then used to propose a model for EF-G−RRF interaction on the ribosome during the recycling process.

Here we utilize fully functional fluorescent derivatives of both RRF and EF-G to carry out the first kinetically resolved study of RRF, EF-G, and thiostrepton interactions on the ribosome. These measurements, along with related equilibrium measurements, permit formulation of a minimal kinetic scheme that accounts quantitatively for such interactions. Our results lead to the following principal conclusions. (1) RRF and EF-G*GDPCP each form binary complexes with the ribosome in two-step reactions, in which an initially formed complex is followed by a more stable complex. (2) Added EF-G*GDPCP both destabilizes and labilizes binding of RRF to the ribosome via formation and breakdown of mixed ternary complexes. (3) Added thiostrepton slows initial binding of EF-G, and prevents both formation of the more stable EF-G complex and EF-G-induced RRF dissociation. (4) Both RRF and EF-G*GDPCP are capable of forming 2:1 complexes with the ribosome. Below we present the results leading to these conclusions, and discuss their implications for the mechanism of disassembly of the post-termination complex.

MATERIALS AND METHODS

Buffers and Materials

Binding and kinetics experiments were conducted in FB buffer, 50 mM Tris-HCl (pH 7.5 at 25 °C), 30 mM KCl,

† This work was supported by NIH Grants GM53146 (B.S.C.), GM071014 (B.S.C.), and GM60429 (A.K.) and by the Creative Biomedical Research Fund (A.K.).

* To whom correspondence should be addressed. Telephone: (215) 898-6330. Fax: (215) 898-2037. E-mail: cooprman@pobox.upenn.edu.

‡ Department of Chemistry.

§ Department of Microbiology, School of Medicine.

[1] Abbreviations: CPM, 7-(diethylamino)-3-(4′-maleimidylphenyl)-4-methylcoumarin; CPS, 7-(diethylamino)-3-(4′-succinimidylphenyl)-4-methylcoumarin; EF-G, elongation factor-G; GDPCP, GTP analogue in which the β- and γ-phosphates are bridged by a CH_2 group; RRF, ribosome recycling factor; ThS, thiostrepton; EF-G*GDPCP, elongation factor-G bound to GDPCP; EF-G-216-CPS*GDPCP, EF-G-216-CPS bound to GDPCP.

10.1021/bi048927p CCC: $27.50
Published on Web 09/17/2004

and 10 mM $MgCl_2$, unless otherwise specified. Storage buffer consists of 50 mM Tris-HCl (pH 7.6), 100 mM KCl, 10 mM $MgCl_2$, 1 mM dithiothreitol, and 15% glycerol. Tightly coupled ribosomes were prepared from *Escherichia coli* MRE600 cells as described previously (*20*), except in the last step ribosome pellets were resuspended in FB buffer. *E. coli* RRF was prepared as described previously (*18*). The RRF concentration was determined by the Bradford assay (*21*) using a bovine serum albumin standard and multiplying by a correction factor (0.73) for the color yield, which was determined by quantitative amino acid analysis of RRF total hydrolysate. Clones for C-terminally His-tagged *E. coli* EF-G and for its triple variant (C113D/C265A/C397S) were provided by K. Wilson and H. Noller (University of California, Santa Cruz, CA). The C16S-RRF variant was also provided by H. Noller. The quadruple EF-G variant (C113D/C265A/C397S/E216C) was provided by J. van Dijk and Y. Goldman (University of Pennsylvania). EF-G proteins were purified on a Ni−NTA (Qiagen) column as described previously (*22*). Eluted protein was concentrated and buffer-exchanged with storage buffer using a Centricon-30 concentrator (Millipore). The EF-G concentration was determined by the Bradford assay (*21*) using a bovine serum albumin standard, which gave values virtually identical to those obtained when ϵ_{280} is set to 62 200 M^{-1} cm^{-1} (*23*). 7-Diethylamino-3-(4′-maleimidylphenyl)-4-methylcoumarin **(**CPM**)** was obtained from Molecular Probes.

Preparation of CPS-Labeled Proteins

RRF-CPS. Labeling reactions were performed in subdued light. RRF (50 μM, 1 mg/mL) and CPM (500 μM, added from a 5 mM solution in DMSO) were incubated in 50 mM Tris-HCl (pH 7.5) and 50 mM KCl at room temperature for 12 h in a reaction vessel covered with aluminum foil. Agitation was provided by an end-over-end mixer/shaker to counter CPM precipitation. The reaction was terminated by adding 2-mercaptoethanol to a final concentration of 10 mM. Precipitated material was removed by filtration through a 0.1 μm membrane filter (Millipore). Excess dye was removed by gel filtration (PD-10, Amersham) followed by several cycles of concentration and exchange with FB buffer using a Centricon-10 concentrator (Millipore). Labeled protein had a stoichiometry of 1.03 CPS/protein, calculated using an $\epsilon_{390,CPS}$ of 27 000 M^{-1} cm^{-1} (*24*).

EF-G-216-CPS. Labeling of C113D/C265A/C397S/E216C-EF-G (14 μM, 1 mg/mL) with CPM (1 mM) in 50 mM Tris-HCl (pH 7.5), 100 mM KCl, and 10% DMSO proceeded similarly, except that reaction was more rapid (30 min, room temperature). The labeled protein, purified as described above, had a stoichiometry of 1.05 CPS/protein.

Assays of RRF Activity

RRF and RRF-CPS binding to 70S ribosomes following incubation for 5 min at 37 °C and for 30 min at 25 °C was quantified using Microcon 100 (Millipore) filtration, in which the amount of bound RRF was determined by Western blotting as described previously (*9*). RRF- or RRF-CPS-induced conversion of polysomes to monosomes was performed as described previously (*9*).

Single-Turnover GTPase

Quenched-flow experiments were carried out at 37 °C using a Kintek apparatus. Final concentrations in 50 mM Tris-HCl (pH 7.5, 25 °C), 70 mM NH_4Cl, 30 mM KCl, 7 mM $MgCl_2$, and 1 mM dithiothreitol were as follows: 0.8 μM EF-G (or EF-G derivative), 0.8 μM ribosomes, and 5 μM GTP.

Equilibrium Fluorescence Measurements

Fluorescence spectra at 25 °C were acquired using SPEX (Fluorolog-3, Instrument S.A., Inc.) with excitation at 395 nm. Solutions were incubated at 37 °C for 5 min and at 25 °C for 30 min before spectra were recorded. All spectra were corrected for small contributions from fluorescence and/or light scattering of ribosomes and, as appropriate, unlabeled proteins and thiostrepton. Inner filter effect corrections were made as described previously (*25*). Equilibrium constants were obtained by fitting equilibrium fluorescence measurements using IGOR Pro (WaveMetrics, Inc.). K_{IF}, the apparent K_d for the 1:1 ribosome−RRF-CPS complex (Figure 1A), was determined by fitting of eq 1

$$[F]_b = \frac{[F]_t + [R]_t + K_{IF} - \sqrt{([F]_t + [R]_t + K_{IF})^2 - 4[F]_t[R]_t}}{2} \quad (1)$$

where $[R]_t$ is the total ribosome concentration, $[F]_t$ is the total RRF-CPS concentration, and $[F]_b$ is the ribosome−RRF-CPS concentration.

Values of $[F]_b$ were obtained from eq 2

$$[F]_b = (F_c - f_u[F]_t)/(f_b - f_u) \quad (2)$$

where f_u and f_b are the specific fluorescence intensities of RRF-CPS in the unbound and bound states, respectively, and F_C is the inner filter effect-corrected fluorescence measured as $[R]_t$ is varied.

Values for K_{IG}, the apparent K_d for the 1:1 ribosome·EF-G-216-CPS−GDPCP complex in the absence and presence of thiostrepton (Figure 3B) were obtained similarly.

Values of K_5-K_{11} were determined by globally fitting the results in Figure 4 to Scheme 3, using the values of K_1-K_4 determined from the results presented in Figures 1, 3, 5, and 6 and the constraints imposed by three thermodynamic cycles (eqs 3a−3c).

$$K_9 = K_8/K_2 \quad (3a)$$

$$K_{11} = K_{10}/K_4 \quad (3b)$$

$$\frac{K_5K_1}{K_2K_6} = \frac{K_7K_3}{K_4} \quad (3c)$$

Stopped-Flow Measurements

Stopped-flow fluorescence emission traces at 25 °C were acquired using an Applied Photophysics SX.18MV stopped-flow spectrofluorometer with excitation at 395 nm. Emission was monitored using a 455 nm long pass filter (Thermo Oriel). All concentrations specified in the figure legends refer to final concentrations in the mixing chamber. At least five independent fluorescence traces were averaged for each reported result.

Analysis of Stopped-Flow Data. In all fittings, the background fluorescence and/or light scattering of ribosome alone

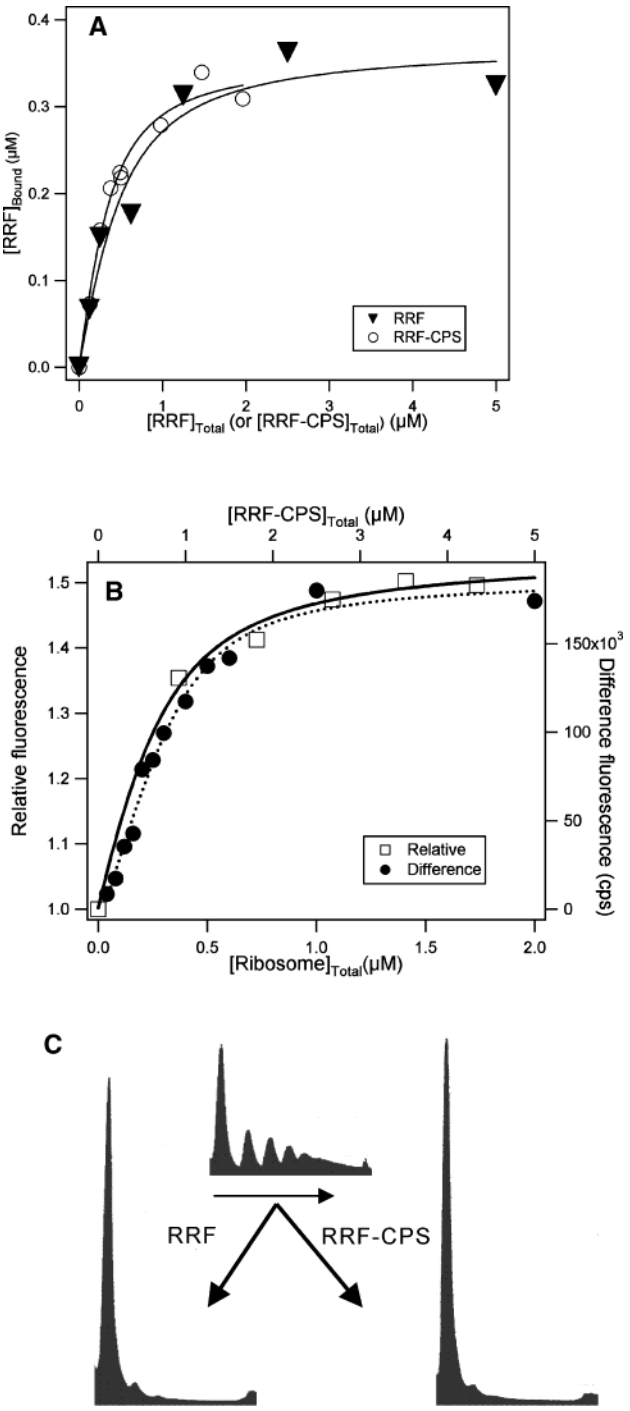

FIGURE 1: Functional activity of RRF-CPS. (A) Binding to ribosomes as measured by the Microcon 100 method with 0.25 μM ribosomes. (B) Binding to ribosomes as measured by the change in fluorescence of RRF-CPS at 470 nm. Results with a fixed ribosome concentration of 1.0 μM (right and top axes, ●) represent the difference in fluorescence intensity due to binding of RRF-CPS to the ribosome and are fit with a K_d of 0. 17 μM (—). Results with a fixed RRF-CPS concentration of 0.26 μM (left and bottom axes, □) represent the relative ratio of fluorescence intensity as a function of ribosome concentration, and are fit with a K_d of 0.13 μM (···). (C) Breakdown of the polysome to monosomes. The reaction mixture contained 4.9 μM EF-G, 363 μM GTP, 50 μM puromycin, 8.2 mM magnesium sulfate, 0.6 A_{260} unit of polysomes, and RRF as indicated: (top) no RRF, (left) 3.6 μM RRF, and (right) 3.6 μM RRF-CPS. The reaction mixture was incubated at 30 °C for 15 min and then centrifuged through a 15 to 30% sucrose gradient in a Beckman SW 50.1 rotor. The *Y*-axis is A_{260}, and the *X*-axis is the fraction number. The horizontal arrow indicates the direction of sedimentation.

(with or without unlabeled protein, with or without thiostrepton as appropriate) was measured separately in the stopped-flow instrument and subtracted from the experimental traces.

Binary Systems. Apparent rate constants for the biphasic binding of RRF-CPS or EF-G-216-CPS*GDPCP to the ribosome (Figures 5 and 6) were determined by fitting fluorescence data to eq 4 in which $F(t)$ is the fluorescence at time t, F_∞ is the fluorescence at the end of the reaction, and ΔF_1 and ΔF_2 are the changes in fluorescence during the first and second phases of the reaction, respectively. Fits for monophasic binding of EF-G-216-CPS*GDPCP to the ribosome in the presence of thiostrepton (Figures 6A and 7B) were performed setting ΔF_2 equal to zero.

$$F(t) = F_\infty + \Delta F_1 e^{-k_{app1}t} + \Delta F_2 e^{-k_{app2}t} \quad (4)$$

Individual rate constants (k_1—k_{-2} and k_3—k_{-4}) were calculated by globally fitting the results (Figures 5 and 6) to the following two-step binding model, in which A is the fluorescent factor and B is the ribosome, and are presented in Table 1.

$$A + B \rightleftharpoons C \rightleftharpoons D$$

Relative fluorescence values for species C and D (i.e., RF_{a1}, RF_{a2}, RG_{m1}, and RG_{m2}) were calculated setting the value for A equal to 1, and are presented in Table 2.

Global Fitting to Scheme 3. Microscopic rate constants were determined by globally fitting stopped-flow kinetic data in Figures 7 and 8 to Scheme 3, using the independently determined equilibrium (K_5—K_{11}) and rate (k_1—k_{-4}) constants as constraints and the program Scientist (MicroMath Research, LC). Stopped-flow fluorescence traces were fit to eq 5

$$F(t) = \sum_i F_i[\mathrm{I}] \quad (5)$$

where F_i is the specific relative fluorescence of each fluorescent species I in solution containing RRF-CPS or EF-G-216-CPS and the relative fluorescence of RRF-CPS or of EF-G-216-CPS*GDPCP is taken to be 1.0. Fitted F values for the various complexes relevant to Figures 7 and 8 are presented in Table 2.

Net rate constants were calculated as described previously (*26*).

RESULTS

Protein Labeling with CPM. Wild-type RRF was labeled on its unique Cys residue (Cys 16) to produce RRF-CPS. Proof that labeling occurred only on the Cys residue comes from the Ellman assay (*27*), which gave stoichiometries of 0.94 and 0.013 Cys residue/RRF prior to and following derivatization with CPM, respectively, and from the lack of CPM incorporation when the C16S-RRF variant was reacted in a parallel fashion with CPM. The quadruple EF-G variant containing a single cysteine at postion 216 was also labeled with CPM to a stoichiometry of 1.05 Cys/EF-G, yielding EF-G-216-CPS. The Ellman assay gave stoichiometries of 0.99 and 0.044 Cys residue/EF-G prior to and following derivatization with CPM, respectively.

Equilibrium Binding Studies

Binding (1:1) of RRF-CPS to the Ribosome. Evaluation of K_{IF}. As demonstrated using the filtration binding assay

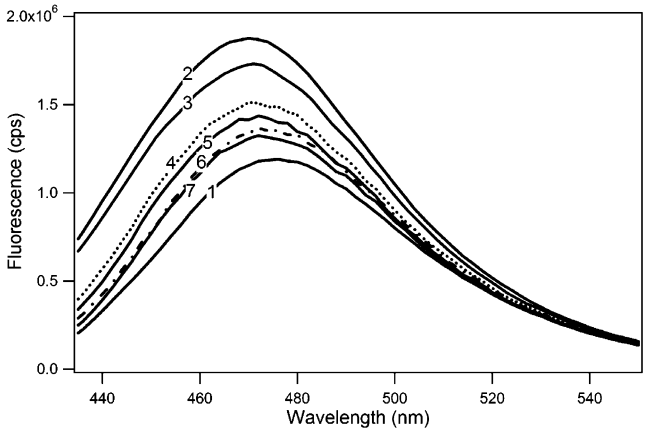

FIGURE 2: Binding of RRF-CPS to ribosomes**.** All solutions contained 0.18 μM RRF-CPS (spectrum 1). The solutions for spectra 2−7 had the following additional components: (2) 1 μM ribosome, (3) 1 μM ribosome and 3 μM EF-G, (4) 1 μM ribosome, 3 μM EF-G, and 200 μM GTP, (5) 1 μM ribosome, 3 μM EF-G, and 200 μM GDP, (6) 1 μM ribosome, 3 μM EF-G, and 200 μM GDPCP, and (7) 5.8 μM RRF and 1 μM ribosome. RRF or EF-G was added after addition of RRF-CPS.

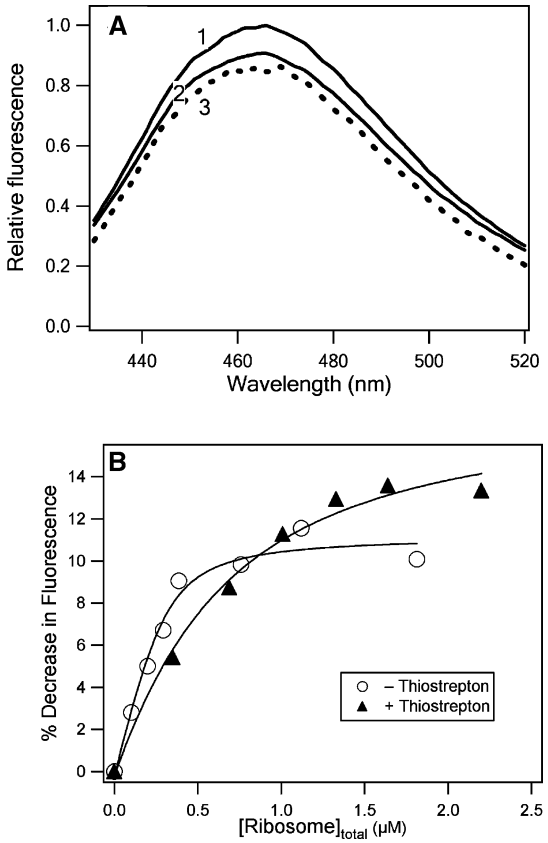

FIGURE 3: Binding of EF-G-216-CPS to ribosomes. (A) Fluorescence of EF-G-216-CPS. All solutions contained 0.3 μM EF-G-216-CPS and 200 μM GDPCP (omission of GDPCP had no effect on spectrum 1). The solutions for spectra 2 and 3 had the following additional components: (2) 1.5 μM ribosomes and (3) 1.5 μM ribosomes and 10 μM thiostrepton (- - -). (B) Fluorescence titration of 0.3 μM EF-G216-CPS and 200 μM GDPCP with ribosomes in the presence and absence of thiostrepton (10 μM). The data represent the difference in fluorescence intensity due to binding of EF-G-216-CPS to the ribosome.

(Figure 1A), RRF-CPS binds to 70S ribosomes with a macroscopic dissociation constant K_{IF} (0.18 ± 0.03 μM) that is virtually the same as that for unmodified RRF (0.26 ± 0.07 μM). These values are essentially identical to those measured elsewhere (*9*, *15*, *28*). RRF-CPS was also as active as RRF in disassembling a model post-termination polysome complex (Figure 1C). These results demonstrate that, compared to unmodified RRF, RRF-CPS binds with essentially unaltered affinity to the high-affinity RRF site on the ribosome.

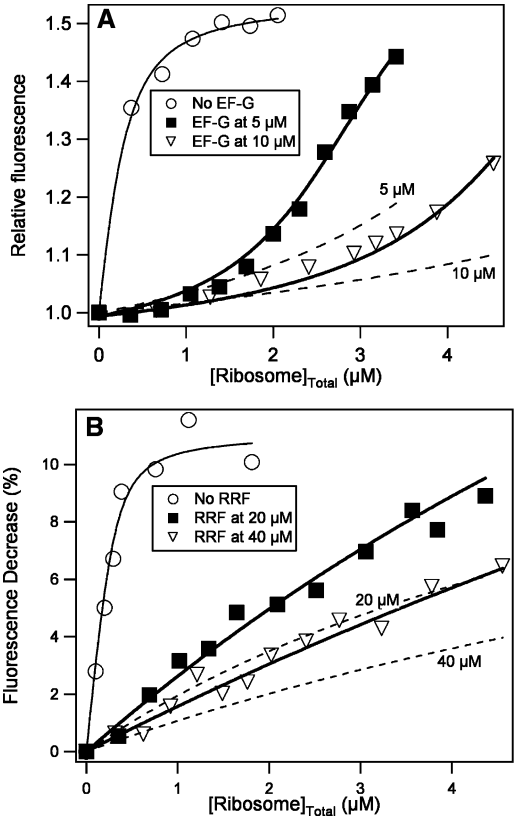

FIGURE 4: Equilibrium measures of RRF and EF-G*GDPCP interaction on the ribosome. (A) Binding of RRF-CPS to ribosomes in the presence of EF-G*GDPCP. The fluorescence of RRF-CPS (0.26 μM) was measured at 470 nm. Measurements were performed following successive addition of ribosomes and EF-G. The curve in the absence of EF-G, repeated from Figure 1B, is shown for comparison. (B) Binding of EF-G-216-CPS*GDPCP to ribosomes in the presence of RRF. The fluorescence of EF-G-216-CPS (0.4 μM) was measured at 470 nm. Measurements were performed following successive addition of ribosomes and RRF. The curve in the absence of RRF is shown for comparison. In panels A and B, the GDPCP concentration was 300 μM. Solid lines through experimental traces are the result of global fitting to Scheme 3, yielding estimates for K_5−K_{11}. Dashed lines are simulations based solely on a competitive interaction between RRF and EF-G for interaction with the ribosome, using the values of K_{IF} (0.2 μM), K_{IG} (0.05 μM), F_{RF*} (1.6), and F_{RG*} (0.88).

The fluorescence spectrum of RRF-CPS shows a small blue shift (from 476 to 468 nm) and a sizable increase (1.6-fold, measured at λ_{max}) on binding to ribosomes (Figure 2). Added unlabeled RRF competes with this binding, nearly restoring the fluorescence spectrum of unbound RRF-CPS (Figure 2). The fluorescence change allowed estimation of a dissociation constant for binding of RRF-CPS to the ribosomes (Figure 1B) of 0.17 ± 0.05 μM. This value is indistinguishable from that determined by filtration (Table 1), when measured by titrating a fixed ribosome concentration with increasing RRF-CPS. A slightly lower value, 0.13 ± 0.03 μM, is obtained when the titration is repeated at a fixed RRF-CPS concentration and an increasing ribosome

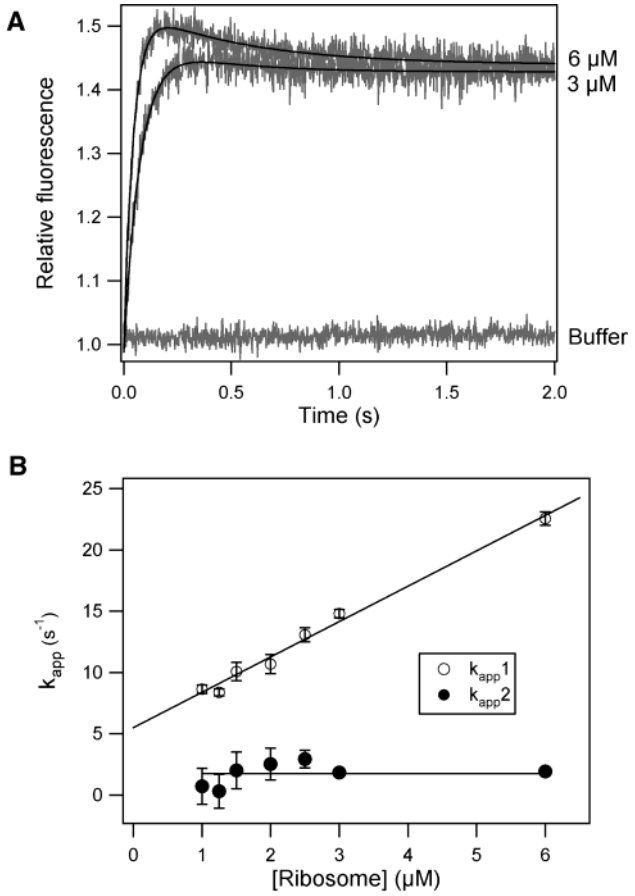

FIGURE 5: Kinetics of RRF-CPS interaction with ribosomes. (A) RRF-CPS (0.22 μM) is rapidly mixed with ribosomes (top trace, 6 μM; bottom trace, 3 μM). Each trace is fit to eq 4. As a control, RRF-CPS is mixed with the binding buffer. (B) Dependence of apparent rate constants on ribosome concentration.

concentration (Figure 1B). This is the more reliable value for the 1:1 complex, since small amounts of the ribosome·$(RRF)_2$ complex (see below) will be formed when RRF is present in excess over ribosomes.

Binding (1:1) of EF-G-216-CPS to the Ribosome. Evaluation of K_{IG}. The fluorescence spectrum of EF-G-216-CPS*GDPCP shows a small decrease in intensity (~10%) on binding to ribosomes (Figure 3A), permitting measurement of a macroscopic dissociation constant K_{IG} for binding of EF-G-216-CPS*GDPCP to ribosomes, 0.053 ± 0.024 μM (Figure 3B), comparable to the value of 0.08 μM previously reported for wild-type EF-G·GDP (*29*). Furthermore, under conditions in which virtually all added EF-G is ribosome-bound, EF-G-216-CPS displays activity in single-turnover, ribosome-dependent uncoupled GTPase ($k_{app} = 57.5 \pm 12.7$ s^{-1}) virtually identical to that of wild-type EF-G ($k_{app} = 59.0 \pm 14.7$ s^{-1}) (data not shown). The latter value is identical to that reported previously (*30*). These results demonstrate that EF-G-216-CPS*GDPCP is functionally identical to EF-G*GDPCP with respect to interaction with a high-affinity site in the ribosome.

EF-G Effect on RRF Binding. As demonstrated in Figure 2, added EF-G·guanosine nucleotide complexes induce substantial reversal of the increase in fluorescence that accompanies binding of RRF-CPS to ribosomes, which we interpret as reflecting release of ribosome-bound RRF-CPS. Measured at a single concentration of EF-G, the extents of

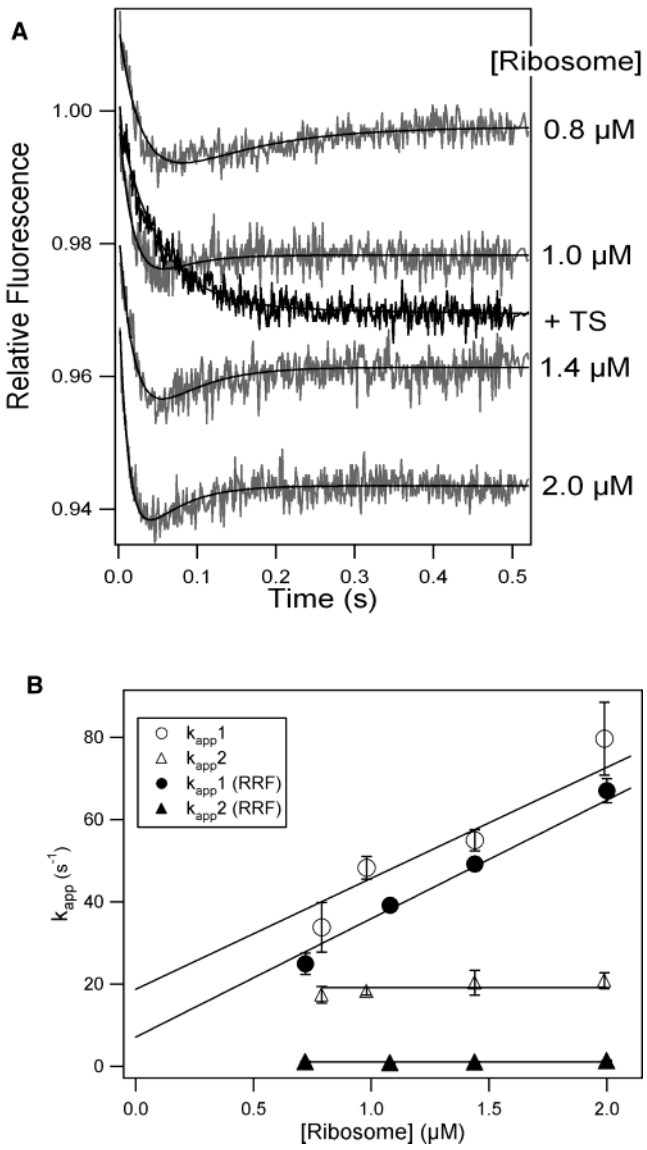

FIGURE 6: Kinetics of EF-G-216-CPS interaction with ribosomes. (A) EF-G-216-CPS (0.1 μM) and GDPCP (100 μM) were rapidly mixed with ribosomes (0.8−2.0 μM). The black trace is for 1.0 μM ribosomes preincubated with 10 μM thiostrepton. Others are shown in gray. Traces in the absence of thiostrepton are fit to eq 4. The trace in the presence of thiostrepton was fit to a single exponential. Traces were offset for clarity relative to 1.0 μM ribosomes by 0.02, −0.02, and −0.04 for 0.8, 1.4, and 2.0 μM ribosomes, respectively. (B) Dependence on ribosome concentration of apparent rate constants for binding of EF-G-216-CPS*GDPCP to ribosomes in the absence (○, △) and presence (●, ▲) of RRF.

release fall in the following order: GDPCP > GDP ~ GTP ≫ no added nucleotide [which agrees with the order determined using the filtration binding assay (*15*)]. These results confirm that GTP hydrolysis is not required for induction of RRF release.

A related set of results is presented in Figure 4A, which also demonstrates that added EF-G*GDPCP decreases the affinity of RRF-CPS for the ribosome. The results obtained show fluorescent changes larger than those predicted by a simple competitive interaction of both factors for the ribosome, based on the values of K_{IF} and K_{IG} determined above, providing evidence for formation of the mixed ternary ribosome·RRF-CPS·EF-G−GDPCP complex (see below).

Table 1: Rate and Equilibrium Constants[a]

rate constants		equilibrium constants	
$k_1 = (3.1 \pm 0.1) \times 10^6\ M^{-1}\ s^{-1}$ $k_{-1} = 1.9 \pm 0.1\ s^{-1}$ $k_2 = 2.2 \pm 0.1\ s^{-1}$ $k_{-2} = 0.6 \pm 0.1\ s^{-1}$	Figure 5	$K_1 = 0.61 \pm 0.04\ \mu M$ $K_2 = k_2/k_{-2} = 3.7 \pm 0.6$ $K_{IF} = K_1/(1 + K_2)$ $=0.26 \pm 0.07\ \mu M$ RRF[b] $=0.18 \pm 0.03\ \mu M$ RRF-CPS[b] $=0.17 \pm 0.05\ \mu M$ RRF-CPS $= 0.13 \pm 0.03\ \mu M$ RRF-CPS	Figure 1A,B
$k_3 = (31 \pm 3) \times 10^6\ M^{-1}\ s^{-1}$ $k_{-3} = 12 \pm 6\ s^{-1}$ $k_4 = 14.3 \pm 1.7\ s^{-1}$ $k_{-4} = 2.4 \pm 0.7\ s^{-1}$	Figure 6A,B	$K_3 = 0.4 \pm 0.2\ \mu M$ $K_4 = k_4/k_{-4} = 6 \pm 2$ $K_{IG} = K_5/(1 + K_6) = 0.053 \pm 0.024\ \mu M$	Figure 3B
$k_5 = (28 \pm 3) \times 10^6\ M^{-1}\ s^{-1}$ $k_{-5} = 82 \pm 9\ s^{-1}$ $k_6 = 2.3 \pm 0.2\ s^{-1}$ $k_{-6} = 1.3 \pm 0.3\ s^{-1}$ $k_7 = (5.7 \pm 2.0) \times 10^6\ M^{-1}\ s^{-1}$ $k_{-7} = 23 \pm 9\ s^{-1}$	Figure 7	$K_5 = 2.9 \pm 1.0\ \mu M$ $K_6 = k_6/k_{-6} = 1.8 \pm 0.7$ $K_7 = 4.0 \pm 1.5\ \mu M$	Figure 4
$k_8 = (3.0 \pm 0.3) \times 10^6\ M^{-1}\ s^{-1}$ $k_{-8} = 16 \pm 3\ s^{-1}$ $k_9 = (2.7 \pm 0.1) \times 10^6\ M^{-1}\ s^{-1}$ $k_{-9} = 3.6 \pm 0.2\ s^{-1}$	Figure 8A,B	$K_8 = 5.3 \pm 1.1\ \mu M$ $K_9 = 1.33 \pm 0.09\ \mu M$ $K_{IIF} = K_8 + K_9 = 6.7 \pm 1.1\ \mu M$	Figure 4
$k_{10} = (10.4 \pm 0.3) \times 10^6\ M^{-1}\ s^{-1}$ $k_{-10} = 3.1 \pm 0.9\ s^{-1}$ $k_{11} = (3.3 \pm 0.3) \times 10^6\ M^{-1}\ s^{-1}$ $k_{-11} = 0.16 \pm 0.02\ s^{-1}$	Figure 8C	$K_{10} = 0.3 \pm 0.1\ \mu M$ $K_{11} = 0.048 \pm 0.007\ \mu M$ $K_{IIG} = K_{10} + K_{11} = 0.35 \pm 0.11\ \mu M$	Figure 4

[a] Values determined from fluorescence measurements, except as otherwise indicated. [b] Determined by a Microcon 100 filtration assay.

Table 2: Relative Fluorescence Values[a] in Equilibrium and Stopped-Flow Experiments

sample[b]	equilibrium[c]	stopped-flow[d]	sample[b]	equilibrium[c]	stopped-flow[d]
F_{F^*}	1.00	1.00	F_{G^*}	1.00	1.00
F_{RF^*}	1.56 ± 0.06		F_{RG^*}	0.88 ± 0.02	
			F_{RG^*ThS}	0.83 ± 0.02	
F_{RF^*a1}		1.62 ± 0.01	F_{RG^*m1}		0.961 ± 0.009
			F_{RG^*mThS}		0.958 ± 0.007
F_{RF^*a2}		1.34 ± 0.01	F_{RG^*m2}		0.983 ± 0.002
F_{RF^*aFb}		1.67 ± 0.01	F_{RG^*m1Gm2}		0.967 ± 0.004
F_{RFaF^*b}		1.47 ± 0.01	F_{RGm1G^*m2}		0.996 ± 0.001
F_{RF^*G}	2.0 ± 0.30		F_{RFG^*}	0.84 ± 0.04	
F_{RF^*a1Gm2}		1.02 ± 0.02	F_{RFa1G^*m2}		0.994 ± 0.001
F_{RF^*a2Gm1}		1.57 ± 0.01	F_{RFa2G^*m1}		0.909 ± 0.003

[a] Indicated by *F*; an asterisk indicates a fluorescently labeled factor. [b] R is ribosome. F is RRF-CPS. G is EF-G*GDPCP. ThS is thiostrepton. [c] Fluorescence measured with a monochromator. [d] Fluorescence measured using a 455 nm long pass filter.

RRF Effect on EF-G Binding. Additional evidence for mixed ternary complex formation is provided by the results presented in Figure 4B, showing that the affinity of EF-G-216-CPS*GDPCP for the ribosome is decreased in the presence of RRF, but again displaying fluorescent changes larger than what is predicted by a simple competitive interaction of both factors for the ribosome.

Kinetic Studies

Kinetics of Binary RRF·Ribosome Complex Formation. The increase in fluorescence intensity upon binding of RRF-CPS to ribosomes provides a tool for following the kinetics of RRF interaction with the ribosome. Sample results, obtained as a function of ribosome concentration (1−6 μM) at a fixed RRF-CPS concentration (0.22 μM), show clear evidence of a biphasic reaction, especially marked at 6 μM ribosomes (Figure 5A), with a rapid large increase followed by a slower, small decrease. As seen in Figure 5B, k_{app1} for the fast phase increases linearly with ribosome concentration, with a slope of 3.0 $\mu M^{-1}\ s^{-1}$, whereas k_{app2} for the slow phase rate constant reaches a maximum value of $\sim$2.5 s^{-1}. Global fitting of these results to reactions 1 and 2 of Scheme 1, in which the initially formed ribosome·RRF_{a1} complex is succeeded by the more stable ribosome·RRF_{a2} complex, yielded values for rate constants k_1-k_{-2} (Table 1). The macroscopic constant calculated from the k_1-k_{-2} values for 1 equiv of RRF binding to the ribosome, K_{IF}, is 0.13 ± 0.03 μM, which agrees perfectly with the equilibrium value determined by fluorescence change under the same conditions (Figure 1B).

Scheme 1. Binding of RRF to the Ribosome

$$R + F \underset{k_{-1}}{\overset{k_1}{\rightleftharpoons}} RF_{a1} \underset{k_{-2}}{\overset{k_2}{\rightleftharpoons}} RF_{a2} \qquad R = \text{ribosome, } F = \text{RRF}$$

Kinetics of Binary EF-G216-CPS·Ribosome Complex Formation. Kinetic studies of binding of EF-G-216-CPS*GDPCP to the ribosome gave results that are strongly formally similar to those obtained with RRF-CPS. Rate measurements as a function of ribosome concentration (0.8−2 μM) at a fixed EF-G-216-CPS concentration (0.1 μM) (Figure 6A) show clear evidence of a biphasic reaction,

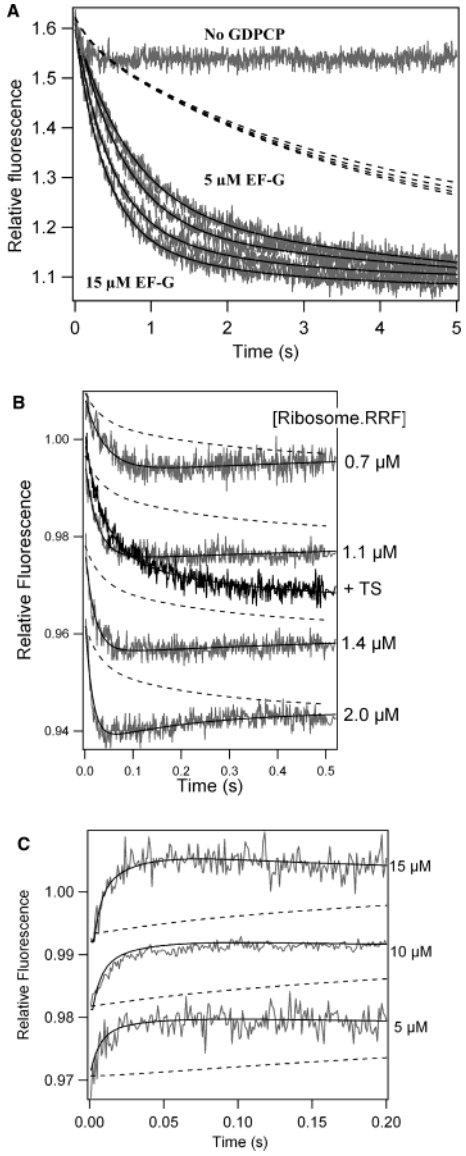

FIGURE 7: Kinetic measures of RRF−EF-G interaction. (A) Rates of EF-G*GDPCP-induced release of RRF-CPS from the ribosome·RRF-CPS complex. The RRF-CPS·ribosome complex, formed by incubating RRF-CPS (0.37 μM) and ribosome (1.5 μM) in binding buffer for 5 min at 37 °C followed by 20 min at 25 °C, was rapidly mixed with EF-G [5 (top), 7 (second), 10 (third), and 15 μM (bottom)] containing GDPCP (200 μM). The top-most trace contained 10 μM EF-G and no GDPCP. (B) Rates of binding of EF-G-216-CPS*GDPCP to ribosomes in the presence of a varying RRF concentration. EF-G-216-CPS (0.12 μM) and GDPCP (100 μM) were rapidly mixed with the ribosome·RRF complex (0.7−2.0 μM, as indicated), formed by preincubating a 1.1-fold excess of RRF with ribosomes in FB buffer for 5 min at 37 °C. The black trace is for 1.1 μM ribosome·RRF complex preincubated with 10 μM thiostrepton. Others are shown in gray. Traces were offset for clarity relative to 1.1 μM ribosomes by 0.02, −0.02, and −0.04 for 0.7, 1.4, and 2.0 μM ribosomes, respectively. (C) Rates of fluorescence change on addition of RRF to ribosome-bound EF-G-216-CPS*GDPCP. EF-G216CPS (0.12 μM) and ribosomes were preincubated with GDPCP (100 μM) and rapidly mixed with various RRF concentrations. Ribosome concentrations were 0.5 μM (5 and 15 μM RRF) and 1.0 μM (10 μM RRF). Traces were offset for clarity relative to 10 μM RRF by −0.01 and 0.01 for 5 and 15 μM RRF, respectively. In panels A−C, solid lines in the absence of thiostrepton are fit to Scheme 3, yielding estimates for k_5-k_{-7}. Dotted lines are simulations assuming that the release or binding of RRF or EF-G*GDPCP proceeds solely via Scheme 1 or Scheme 2, respectively. The trace in the presence of thiostrepton in panel B was fit to a single exponential.

with a rapid large decrease followed by a slower, small increase. As seen in Figure 6B, k_{app1} increases linearly with ribosome concentration, whereas k_{app2} is independent of ribosome concentration. Fitting the data to reactions 3 and 4 of Scheme 2, in which an initially formed ribosome·EF-G-216-CPS$_{m1}$ complex isomerizes to a ribosome·EF-G-216-CPS$_{m2}$ complex, yielded values for the rate constants k_3-k_{-4} (Table 1). The macroscopic constant calculated from the k_3-k_{-4} values for 1 equiv of EF-G-216-CPS binding to the ribosome, K_{IG} (0.087 ± 0.055 μM), is consistent with the equilibrium value determined from the data in Figure 3B.

Scheme 2. Binding of EF-G*GDPCP to the Ribosome

$$R + G \underset{k_{-3}}{\overset{k_3}{\rightleftharpoons}} RG_{m1} \underset{k_{-4}}{\overset{k_4}{\rightleftharpoons}} RG_{m2} \qquad R = \text{ribosome, G = EF-G.GDPCP}$$

Kinetics of RRF and EF-G−GDPCP Interaction on the Ribosome. Addition of increasing amounts of EF-G*GDPCP to a preformed 1:1 ribosome·RRF-CPS complex leads to increasing rates of fluorescence decrease, corresponding to the release of RRF-CPS from the ribosome (Figure 7A). A related set of experiments was carried out by adding EF-G216-CPS*GDPCP to increasing concentrations of a 1:1 ribosome·RRF complex and monitoring the rates of EF-G216-CPS−GDPCP binding by the decrease in fluorescence (Figure 7B). Paralleling the reaction carried out in the absence of RRF (Figure 6A), the binding of EF-G216-CPS*GDPCP in the presence of RRF occurs in a biphasic reaction. k_{app1} increases linearly with ribosome concentration, whereas k_{app2} is independent of ribosome concentration. The two sets of results are compared in Figure 6B, which shows that RRF has little effect on k_{app1} but markedly reduces k_{app2}. In a third experiment (Figure 7C), large excesses of RRF were added to a 1:1 ribosome·EF-G-216-CPS complex, leading to a rapid increase in fluorescence, the rate of which increases as a function of RRF concentration, from 64 ± 11 s^{-1} at 5 μM RRF to 89 ± 5 s^{-1} at 10 μM RRF to 110 ± 13 s^{-1} at 15 μM RRF. Strong kinetic evidence for mixed ternary complex formation is provided by the much faster rates of fluorescence change observed in Figure 7A−C when compared with rates predicted from kinetic pathways in which the release or binding of RRF or of EF-G*GDPCP proceeds solely via Scheme 1 or Scheme 2, respectively.

Kinetic Evidence for Formation of Ribosome·(RRF)$_2$ and Ribosome·(EF-G)$_2$ Complexes. Added unlabeled RRF displaces RRF-CPS from the ribosome (Figure 2). This process, which results in a decrease in fluorescence, proceeds much more rapidly than would be predicted from Scheme 1 (Figure 8A). In a related experiment, adding RRF-CPS to ribosomes which have been preincubated with RRF in excess leads to partial binding of RRF-CPS that is also more rapid than predicted solely from Scheme 1 (Figure 8B). Similarly, addition of excess unlabeled EF-G*GDPCP to the ribosome·EF-G-216-CPS−GDPCP complex leads to an increase in fluorescence (Figure 8C), but at a rate that is far more rapid than that predicted solely from Scheme 2. These observations provide strong evidence that each of the factors can bind to a second site on the ribosome.

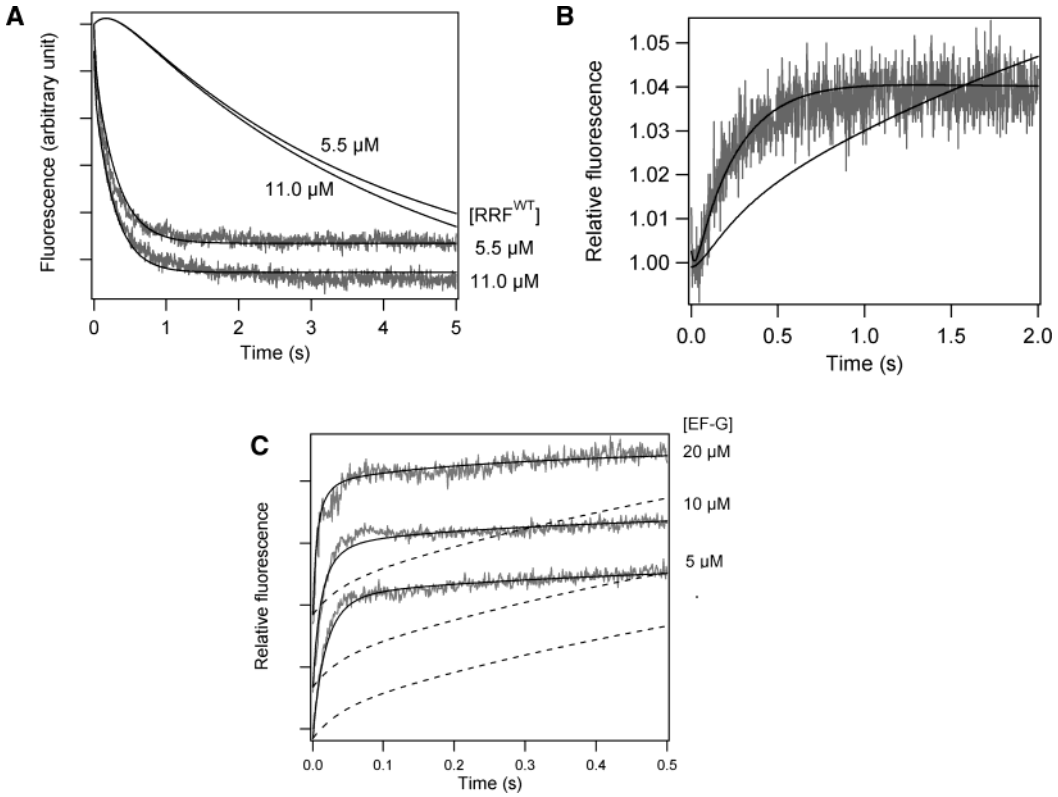

FIGURE 8: Kinetic evidence for the formation of ribosome·$(RRF)_2$ and ribosome·$(EF\text{-}G*GDPCP)_2$ complexes. (A) Rate of release of RRF-CPS from ribosomes on addition of excess RRF. RRF-CPS (0.37 μM) was preincubated with ribosomes (1.5 μM) and rapidly mixed with unlabeled RRF (5.5 and 11 μM) in the stopped-flow apparatus. (B) Rate of binding of RRF-CPS to ribosomes in the presence of excess RRF. RRF-CPS (0.37 μM) was rapidly mixed with preincubated ribosomes (1.5 μM) and RRF (5.5 μM). In panels A and B, solid lines through experimental traces are the result of global fitting to Scheme 3, whereas solid lines that deviate from the experimental traces are the results of simulation considering steps 1 and 2 only. (C) Release of ribosome-bound EF-G-216-CPS by added EF-G. EF-G-216-CPS (0.1 μM) and ribosomes (1.0 μM) were preincubated with GDPCP (100 μM) and rapidly mixed with different concentrations of EF-G. Traces were offset for clarity relative to 10 μM EF-G by -0.01 and 0.01 for 5 and 20 μM EF-G, respectively. Solid lines through experimental traces are the result of global fitting to Scheme 3. Dashed lines are the results of simulation considering steps 3 and 4 only.

Thiostrepton Effects

Thiostrepton (10 μM) affects both the thermodynamics and kinetics of EF-G−GDPCP interaction with the ribosome. Binding of EF-G-216-CPS*GDPCP to the ribosome in the presence of thiostrepton leads to a somewhat larger decrease in fluorescence intensity (~14% vs 10%, Figure 3A) and a 10-fold decrease in apparent affinity (Figure 3B). With respect to the kinetics of EF-G-216-CPS−GDPCP binding, preincubation of ribosomes with thiostrepton decreases the apparent rate constant of the first phase from 48 $\pm$ 3 to 15.6 $\pm$ 0.3 s^{-1} and abolishes the second phase (Figure 6A). Thus, the effect of thiostrepton in weakening binding of EF-G-216-CPS*GDPCP to the ribosome appears to be linked to its preventing conversion of an initially formed complex, which we denote RG_mThS, into a more stable complex. The essential identity in the values of K_3 and of the EF-G−GDPCP dissociation constant in the presence of thiostrepton [0.4 $\pm$ 0.2 and 0.49 $\pm$ 0.14 μM (Figure 3B), respectively], and the similarity of F_{RG*m1} and $F_{RG*mThS}$ (Table 2), suggest that EF-G may be in a similar location in the RG_{m1} and RG_mThS complexes. Thiostrepton has similar effects on the kinetics of binding of EF-G-216-CPS*GDPCP to ribosomes preincubated with 1 equiv of RRF (Figure 7B), i.e., decreasing the apparent rate constant of the first phase from 39 $\pm$ 1 to 10.5 $\pm$ 0.2 s^{-1}, resulting in the formation of RF_aG_mThS, and abolishing the second phase.

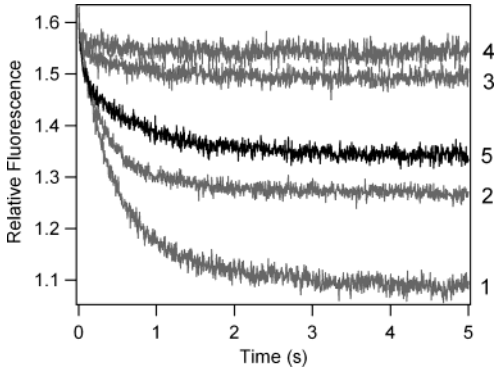

FIGURE 9: Effect of thiostrepton on EF-G*GDPCP-induced release of RRF-CPS from the ribosome·RRF-CPS complex. Increasing amounts of thiostrepton (0, 0.5, 3, and 20 μM, traces 1−4, respectively, gray) were preincubated with RRF-CPS (0.37 μM) and ribosomes (1.5 μM) and then rapidly mixed with EF-G (10 μM) containing GDPCP (200 μM). Alternatively, 20 μM TS was preincubated with EF-G*GDPCP (trace 5, black) and then rapidly mixed with RRF-CPS (0.37 μM) and ribosomes (1.5 μM).

The effect of thiostrepton on the rate and extent of RRF-CPS release induced by EF-G*GDPCP (Figure 9) depends both on the thiostrepton:ribosome ratio (traces 1−4) and on the order of addition (traces 4 and 5). Preincubation of the RRF-CPS·ribosome complex with thiostrepton at a thiostrepton:ribosome ratio of <1 led to an only partial release of RRF-CPS, although with a rate constant identical to that seen in the absence of thiostrepton, whereas prein-

cubation at a ratio of >2 led to a complete blockage of release. These results demonstrate that prebinding of thiostrepton to its 50S site prevents EF-G*GDPCP from binding in a manner inducing expulsion of RRF from the ribosome. Further, simultaneous addition of EF-G*GDPCP and excess thiostrepton to the ribosome·RRF-CPS complex led to both a partial release of RRF and a decreased rate constant for such release, indicating that EF-G and thiostrepton compete kinetically for binding to an overlapping site on the ribosome.

DISCUSSION

A Minimal Kinetic Scheme for RRF and EF-G Interaction on the Ribosome

A minimal kinetic scheme accounting quantitatively for the binding and rate data presented above must accommodate the following observations and inferences from this work. (1) RRF and EF-G*GDPCP weaken each other's binding to the ribosome and form at least one ternary complex with the ribosome (Figures 4 and 7). (2) RRF and EF-G*GDPCP each bind to the ribosome in two-step reactions (Figures 5 and 6). (3) Thiostrepton blocks both the second step of EF-G*GDPCP binding and EF-G*GDPCP-induced release of ribosome-bound RRF. (4) Both RRF and EF-G*GDPCP can form 2:1 complexes with the ribosome (Figure 8). It should also accommodate restrictions posed by relevant results from other studies. Scheme 3, which incorporates Schemes 1 and 2 and has a total of 11 reversible steps, meets these criteria, as discussed below.

Scheme 3. Minimal Model for RRF (F), EF-G*GDPCP (G), and Thiostrepton (ThS) Interaction on the Ribosome (R)

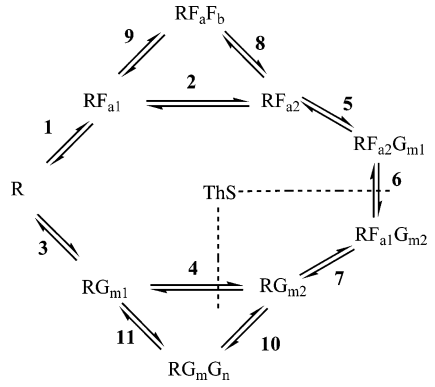

Scheme 3 includes two mixed ternary complexes based on our inability to fit the complete set of results presented in Figure 7 if we included only a single complex. Since each factor forms two 1:1 complexes with the ribosome, there are potentially four mixed ternary complexes to consider. Results from cryoelectron microscopy and chemical cross-linking studies (*31*) indicate that the positions of RRF within its more stable binary complex (i.e., RF_{a2} in Scheme 1) have a direct steric overlap with EF-G*GDPCP in its more stable binary complex (i.e., RG_{m2} in Scheme 2), effectively excluding a ternary complex of the form $RF_{a2}G_{m2}$. The ternary complexes included in Scheme 3, $RF_{a2}G_{m1}$ and $RF_{a1}G_{m2}$, each have one of the factors binding in its more stable form. We excluded the complex $RF_{a1}G_{m1}$ from consideration both because only two ternary complexes were needed to fit the data and because, with each of the factors binding in its less stable form, it was unlikely to be present in large amounts. Consistent with the choice of $RF_{a2}G_{m1}$ and $RF_{a1}G_{m2}$ as the two ternary complexes are the similarities in the fitted rate constants for k_1 [$(3.1 \pm 0.1) \times 10^6$ M^{-1} s^{-1}] and k_7 [$(5.7 \pm 2.0) \times 10^6$ M^{-1} s^{-1}], both measuring initial binding of RRF to the ribosome, and for k_3 [$(31 \pm 3) \times 10^6$ M^{-1} s^{-1}] and k_5 [$(28 \pm 3) \times 10^6$ M^{-1} s^{-1}], both measuring initial binding of EF-G*GDPCP to the ribosome.

A second feature of Scheme 3 is the strong inhibition of reactions 4 and 6 by thiostrepton, indicated by the dotted lines. Each of these reactions involves the conversion of G_{m1} to G_{m2}, leading to the conclusion that the binding of thiostrepton to its site on the ribosome between ribosomal L11 and parts of 23S rRNA helix 44 (*32*) directly interferes with this conversion. Furthermore, the results presented in Figure 9 indicate that EF-G and thiostrepton compete kinetically for binding to an overlapping site on the ribosome.

The third notable feature of Scheme 3 is the inclusion of the 2:1 ribosome·$(RRF)_2$ and ribosome·$(EF\text{-}G*GDPCP)_2$ complexes. For RRF, this is in accord with prior results of Kiel *et al*. (*15*), demonstrating two ribosome binding sites for this factor. Moreover, there is clear structural mimicry between tRNA and RRF (*33*) and tRNA can bind to at least three sites on the ribosome. Notwithstanding the similar mimicry between domain IV of EF-G and tRNA (*34*, *35*), formation of a ribosome·$(EF\text{-}G*GDPCP)_2$ complex was unanticipated, given EF-G's large volume and well-defined binding site, and the generally accepted value of one EF-G per ribosome in the bacterial cell (*36*). However, it must be emphasized that, given the paucity of available binding data for EF-G, there is absolutely no evidence in the literature ruling out a 2:1 EF-G complex, and the EF-G:ribosome ratio has been reported to increase to a value of 2 during the transition from the exponential to stationary phase (*37*). Furthermore, the evidence for formation of both 2:1 complexes from our present results is rather strong. We have already noted the kinetic evidence (Figure 8). The binding results displayed in panels A and B of Figure 4 also support this notion, as it was not possible to fit these results solely on the basis of the complexes depicted in the central loop (reactions 1−7) of Scheme 3. By contrast, excellent fits were obtained when the 2:1 complexes were included. It is noteworthy that the initial slope in Figure 4A is near zero, indicating that essentially no RRF-CPS is bound to the ribosome when $[EF\text{-}G]_t \gg [\text{ribosome}]_t$, i.e., when the ribosome is saturated with EF-G. This result provides a strong indication that RRF cannot bind to ribosomes containing two bound EF-Gs; i.e., the quaternary complex, ribosome·RRF·$(EF\text{-}G*GDPCP)_2$, is not formed.

The inclusion of two-site factor binding in Scheme 3, which describes interaction with bare ribosomes, raises the question of whether second-site binding could have biological importance. On one hand, it is likely that bound tRNAs and other factors that mimic tRNAs (*4*) will strongly compete for such secondary site RRF or EF-G binding, reducing its importance during elongation. On the other hand, part of the mechanism of ribosome recycling involves interaction of RRF and EF-G with 70S ribosomes devoid of tRNA (Figure 10), where secondary site interaction could be important, especially since EF-G and RRF concentrations in the cell can exceed K_{IIG} [~40-fold (*38*)] and K_{IIF} [~3-fold (*39*)], respectively.

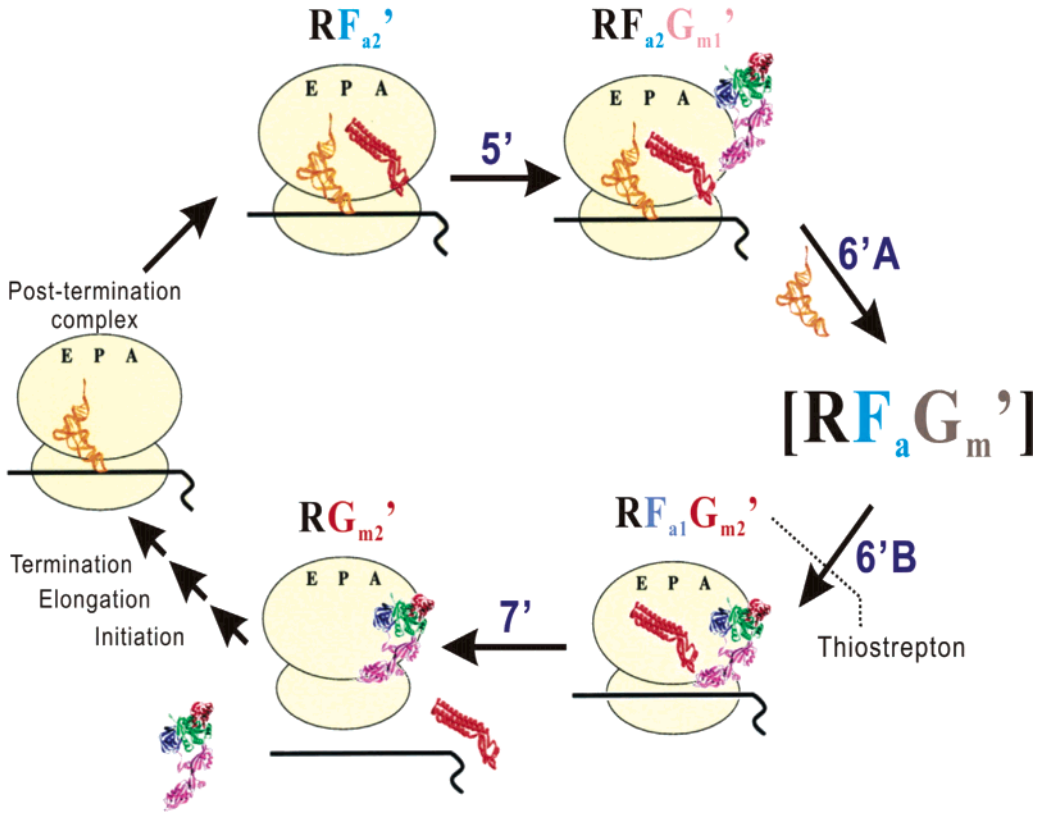

FIGURE 10: Model for RRF−EF-G interaction during ribosome recycling. Complexes RF_{a2}, $RF_{a2}G_{m1}$, and $RF_{a1}G_{m2}$ correspond precisely to complexes a−c in the model of Kiel *et al.* (*15*). Steps 5′−7′ refer to Scheme 3. Step 6′ is divided into two steps for physiological complexes (see the Discussion). Step 6′B is inhibited by thiostrepton, as indicated by the blocking line.

An important ambiguity in Scheme 3 concerns the relationship, if any, between the two steps seen in the kinetics of factor binding experiments (Schemes 1 and 2) and the two sites of binding invoked for each factor; i.e., RRF_{a1} and RRF_{a2} may correspond to two conformations of RRF bound to essentially the same site, or to RRF binding to two distinct sites, and similarly for EF-G*GDPCP$_{m1}$ and EF-G*GDPCP$_{m2}$. The results presented in this work do not permit a clear choice between these possibilities. However, we favor a model in which RF_{a1} and RF_{a2} correspond to binding of RRF to two distinct sites (see ref *15*), and RG_{m1} and RG_{m2} correspond to two conformations of EF-G bound in two locations that are strongly overlapping, based on cryoelectron microscopy studies of binding of EF-G to the ribosome (*40*, *41*).

Scheme 3 also contains certain simplifications, which are justified in the context of presenting a minimal model, but which are not necessarily correct in detail. Thus, the interconversion of the two mixed ternary complexes, which in Scheme 3 proceeds directly via reaction 6, may in fact proceed via intermediates or via factor dissociation and reassociation. In addition, Scheme 3 does not consider the quaternary complex $RF_aF_bG_{m1}$, despite the lack of direct evidence against its formation, since it is not required to fit the results that were obtained. However, it is likely that such a complex would form to at most a minor extent.

Quantitative Conclusions from Scheme 3 and Table 1. The nine species in Scheme 3 are linked by 11 equilibrium constants (K_1−K_{11}), of which eight are independent, and 22 rate constants (k_1−k_{11} and k_{-1}−k_{-11}), values of which are presented in Table 1. These values permit several quantitative conclusions with respect to both the equilibria and kinetics of RRF and EF-G interaction with the ribosome.

First, the presence of EF-G*GDPCP weakens binding of RRF to the ribosome by 20-fold, and vice versa. This is demonstrated by comparing the apparent dissociation constants from the 1:1:1 ribosome·RRF·EF-G*GDPCP complex for RRF [$K_F^G = 3.0\ \mu$M (eq 6a)] and EF-G*GDPCP [$K_G^F = 1.3\ \mu$M (eq 6b)] with the values of K_{IF} (0.13 μM) and K_{IG} (0.055 μM), respectively. This conclusion is consistent with results reported by Kiel *et al.* (*15*), indicating a >10-fold reduction in RRF affinity in the presence of EF-G.

$$K_G^F = \frac{K_7\left(1 + \frac{1}{K_4}\right)}{1 + K_6} \tag{6a}$$

$$K_F^G = \frac{K_5\left(1 + \frac{1}{K_2}\right)}{1 + \frac{1}{K_6}} \tag{6b}$$

Second, the value of the equilibrium constant for interconversion of the two ternary complexes, K_6, is just over 1 (1.8 ± 0.7); i.e., the two complexes are essentially isoenergetic.

Third, the dissociation constant for RRF from the ribosome·$(RRF)_2$ complex ($K_{IIF} = 6.7\ \mu$M) is 20-fold higher than the dissociation constant for EF-G*GDPCP from the ribosome·$(EF\text{-}G^*GDPCP)_2$ complex ($K_{IIG} = 0.35\ \mu$M). The comparatively weak second site binding of RRF accounts for the failure of RRF added at 5.8 μM to remove all bound

RRF-CPS from the ribosome (Figure 2); if there were only a single, high-affinity site for RRF, virtually all of the RRF-CPS would have been removed.

Fourth, binding of EF-G*GDPCP to form the mixed ternary complex not only destabilizes RRF binding in a thermodynamic sense, as discussed above, but also substantially increases the lability of RRF binding. Thus, the net rate constant for EF-G-induced RRF release via steps 5−7 increases from 1.3 to 1.7 s^{-1}, as the EF-G*GDPCP concentration is increased from 5 to 15 μM, which is 6−8 times faster than the net rate constant for RRF release via a reversal of steps 1 and 2 (0.22 s^{-1}). As the estimated *in vivo* concentration of EF-G is ~20 μM (*38*), the pronounced effect of added EF-G*GDPCP in increasing bound RRF lability is likely to be physiologically relevant.

Fifth, in contrast, although ribosome-bound RRF destabilizes EF-G binding in a thermodynamic sense, it has little effect on the lability of bound EF-G*GDPCP. In the absence of RRF, EF-G*GDPCP release proceeds by reversal of steps 3 and 4, with a net rate constant of 1.0 s^{-1}. Addition of RRF provides an alternate route for EF-G*GDPCP dissociation via steps 7, 6, and 5, with a net rate constant of 0.7−1.0 s^{-1} as the RRF concentration is increased from 5 to 15 μM, a range which approximates *in vivo* concentrations (*39*).

Sixth, the rapid increase in fluorescence seen upon addition of either RRF (Figure 7C) or EF-G*GDPCP (Figure 8C) to a preformed ribosome·EF-G-216-CPS*GDPCP complex is not due to release of bound EF-G-216-CPS but rather to the formation of the mixed ternary ribosome·RRF·EF-G*GDPCP complex or the 2:1 ribosome·$(EF\text{-}G*GDPCP)_2$ complex, respectively. In these complexes, the fluorescence of bound EF-G-216-CPS*GDPCP is similar to that of free EF-G-216-CPS*GDPCP, so there is little change in fluorescence when EF-G-216-CPS*GDPCP is released from the ribosome.

Relevance of These Results for Ribosome Function

EF-G Interaction with the Ribosome. Although k_3 and k_{-3} are the first reported direct measures of the rate constants for the binding of an EF-G*GTP-like complex to a bare ribosome, Savelsbergh *et al*. (*42*) have reported rate constants for binding of EF-G*GTP and an EF-G*GTP analogue to pretranslocation ribosomes containing fMetPhe-$tRNA^{Phe}$ in the A-site. Their values for formation of the EF-G*GTP complex, measured indirectly at 37 °C by a change in the fluorescence of the tRNA, were 1.5×10^8 M^{-1} s^{-1} and 140 s^{-1}, 5−10 times faster in each direction than the rate constants we report, measured at 25 °C. Thus, the equilibrium constant for the initial binding of EF-G-216-CPS*GDPCP to the bare ribosome (0.4 ± 0.2 μM) is similar to the corresponding constant for binding of EF-G*GTP to the pretranslocation ribosome (0.9 μM), but the corresponding rate constants may be somewhat lower.

The rate constant for RG_{m1} to RG_{m2} equilibration, 17 s^{-1} at 25 °C, is much slower than the rate constant for ribosome-dependent EF-G*GTPase, but matches well the rate constant of 35 s^{-1} at 37 °C for the so-called "ribosomal unlocking" step that is believed to limit release of P_i from EF-G as well as tRNA−mRNA translocation (*42*). This coincidence suggests that unlocking could be an intrinsic consequence of binding of the EF-G*G-nucleotide complex to the ribosome, and not require GTP hydrolysis as such, consistent with the demonstration that EF-G*GDPCP binding alone induces large conformational changes in the ribosome (*40*, *41*). On the other hand, the rate constant for $RF_{a2}G_{m1}$−$RF_{a1}G_{m2}$ equilibration is much slower (3.6 s^{-1}), and it may be that GTP hydrolysis is required for comparatively rapid EF-G conformational change within a ribosome to which other ligands are bound (i.e., RRF or tRNA/mRNA).

Post-Termination Complex Disassembly. Steps 5−7 in Scheme 3 correspond to EF-G stimulation of RRF release, which is an important part of the post-termination complex disassembly process. The net rate constant for this process at physiologically reasonable concentrations of EF-G is ~1.5 s^{-1} at 25 °C, which should correspond to a value of 3−4 s^{-1} at 37 °C. This is compatible with an estimated overall rate constant for *in vivo* ribosome recycling of 0.7 s^{-1} at 37 °C (*43*, *44*).

Kiel *et al*. (*15*) have proposed a model for EF-G−RRF interactions during the disassembly process, using binding data obtained for post-termination ribosome complexes. Importantly, they showed that such interactions on bare ribosomes were similar. Moreover, the RRF binding site appears to be similar in both bare ribosomes and ribosomes with bound mRNA and bound tRNA at the P/E site (*31*, *45*). These considerations make it both worthwhile and valid to place the results of our work in the context of the Kiel *et al*. model, as in Figure 10. In discussing Figure 10, we refer to the known A, P, E, and hybrid (A/P, P/E) sites for tRNA binding (*46*), and note the use of primes to designate complexes and reactions of post-termination ribosomes that we are comparing to complexes and reactions of bare ribosomes.

Beginning with the post-termination complex, the first step in Figure 10 involves the binding of RRF to form the RF_{a2}' complex. There is strong evidence that RF_{a2} in Scheme 3 corresponds to binding of RRF to the A/P site (*9*, *10*, *28*, *31*, *45*), and we speculate that RF_{a1} corresponds to binding of RRF to the P/E- or E-site (see below). As this latter site is blocked in the post-termination complex, we infer that RRF uses an alternative route to form the RF_{a2}' complex. The second step (step 5′) proceeds in a manner that is an exact analogy to step 5, resulting in formation of the mixed ternary complex $RF_{a2}G_{m1}'$.

Steps 6A′ and 6B′ correspond to a movement whereby $RF_{a2}G_{m1}'$ is converted to $RF_{a1}G_{m2}'$. Conversion of the $RF_{a2}G_{m1}'$ complex to $RF_{a1}G_{m2}'$ is depicted as taking place in two steps (steps 6A′ and 6B′) via formation of intermediate RF_aG_m'. Step 6A′ corresponds to the release of tRNA, which is almost unaffected by thiostrepton, whereas step 6B′ corresponds to the conversion of G_{m1} to G_{m2}, which is inhibited by thiostrepton (*15*), and the movement of RRF to the F_{a1} site, which is now available because of tRNA release. We posit that RF_aG_m' has a structure analogous to that of RF_aG_mThS, the ternary complex formed in the presence of thiostrepton which is unable to proceed to $RF_{a1}G_{m2}$ (Figure 7B). The existence of an intermediate RF_aG_m between $RF_{a2}G_{m1}$ and $RF_{a1}G_{m2}$ that is stabilized by thiostrepton is consistent with the results of Rodnina *et al*. (*30*), showing that while thiostrepton does not interfere with the rapid GTP hydrolysis that follows initial EF-G*GTP binding it does inhibit P_i release, as well as with recent evidence from binding studies (*15*). On the other hand, the thiostrepton effects we observe here run counter to the conclusion of

Cameron *et al*. (*47*) that thiostrepton prevents EF-G*GTP from binding to the ribosome. However, it is worth pointing out that the results of these latter workers could just as easily have been represented as demonstrating that thiostrepton alters and weakens such binding, which we do observe.

Step 7′ corresponds to the release of RRF from $RF_{a1}G_{m2}'$, in exact analogy with step 7 of Scheme 3. mRNA is depicted as being released simultaneously with RRF, based on recent results of V. S. Raj and A. Kaji (unpublished) and the demonstration by Kiel *et al*. (*15*) that mRNA release follows the translocation step. Last, EF-G dissociates prior to recycling of the bare ribosome. In Scheme 3, in the presence of GDPCP, such dissociation takes place via RG_{m1} or $RG_{m1}F_{a2}$, but in the presence of GTP, it is possible that EF-G could dissociate directly from RG_{m2}' or even from $RG_{m2}F_{a1}'$ as a consequence of GTP hydrolysis.

In summary, we present binding and rate results for RRF, EF-G*GDPCP, and thiostrepton interaction with the ribosome that allow formulation of a minimal kinetic scheme (Scheme 3) accounting quantitatively for these results. The main features of Scheme 3 are (1) RRF and EF-G*GDPCP each form binary complexes with the ribosome in two-step reactions, in which the initial binding step is followed by an isomerization step, (2) RRF and EF-G*GDPCP form at least two interconvertible mixed ternary complexes on the ribosome, (3) the affinity of RRF for the ribosome is decreased and its rate of dissociation is substantially increased in the mixed ternary complex as opposed to the binary complex, (4) EF-G*GDPCP-induced release of RRF is linked to the isomerization step in binding of EF-G*GDPCP to the ribosome, (5) thiostrepton slows initial binding of EF-G*GDPCP and prevents both the isomerization step and EF-G-induced RRF dissociation, (6) the rate constant for EF-G*GDPCP-induced RRF dissociation is compatible with overall rate constant for *in vivo* ribosome recycling, and (7) both RRF and EF-G*GDPCP can form 2:1 complexes with the ribosome which may be biologically relevant.

ACKNOWLEDGMENT

We thank Harry Noller, Kevin Wilson, Juliette van Dijk, and Yale Goldman for providing EF-G and/or RRF variants, and Nora Zuno for excellent technical assistance.

REFERENCES

1. Bashan, A., Agmon, I., Zarivach, R., Schluenzen, F., Harms, J., Berisio, R., Bartels, H., Franceschi, F., Auerbach, T., Hansen, H. A., Kossoy, E., Kessler, M., and Yonath, A. (2003) Structural basis of the ribosomal machinery for peptide bond formation, translocation, and nascent chain progression, *Mol. Cell 11*, 91−102.
2. Frank, J. (2003) Electron microscopy of functional ribosome complexes, *Biopolymers 68*, 223−233.
3. Moore, P. B., and Steitz, T. A. (2003) The structural basis of large ribosomal subunit function, *Annu. Rev. Biochem. 72*, 813−850.
4. Ramakrishnan, V. (2002) Ribosome structure and the mechanism of translation, *Cell 108*, 557−572.
5. Yusupov, M. M., Yusupova, G. Z., Baucom, A., Lieberman, K., Earnest, T. N., Cate, J. H., and Noller, H. F. (2001) Crystal structure of the ribosome at 5.5 Å resolution, *Science 292*, 883−896.
6. Rodnina, M. V., Daviter, T., Gromadski, K., and Wintermeyer, W. (2002) Structural dynamics of ribosomal RNA during decoding on the ribosome, *Biochimie 84*, 745−754.
7. Cassataro, J., Delpino, M. V., Velikovsky, C. A., Bruno, L., Fossati, C. A., and Baldi, P. C. (2002) Diagnostic usefulness of antibodies against ribosome recycling factor from *Brucella melitensis* in human or canine brucellosis, *Clin. Diagn. Lab. Immunol. 9*, 366−369.
8. Cassataro, J., Velikovsky, C. A., Giambartolomei, G. H., Estein, S., Bruno, L., Cloeckaert, A., Bowden, R. A., Spitz, M., and Fossati, C. A. (2002) Immunogenicity of the *Brucella melitensis* recombinant ribosome recycling factor-homologous protein and its cDNA, *Vaccine 20*, 1660−1669.
9. Hirokawa, G., Kiel, M. C., Muto, A., Kawai, G., Igarashi, K., Kaji, H., and Kaji, A. (2002) Binding of ribosome recycling factor to ribosomes, comparison with tRNA, *J. Biol. Chem. 277*, 35847−35852.
10. Hirokawa, G., Kiel, M. C., Muto, A., Selmer, M., Raj, V. S., Liljas, A., Igarashi, K., Kaji, H., and Kaji, A. (2002) Post-termination complex disassembly by ribosome recycling factor, a functional tRNA mimic, *EMBO J. 21*, 2272−2281.
11. Ito, K., Fujiwara, T., Toyoda, T., and Nakamura, Y. (2002) Elongation factor G participates in ribosome disassembly by interacting with ribosome recycling factor at their tRNA-mimicry domains, *Mol. Cell 9*, 1263−1272.
12. Janosi, L., Mottagui-Tabar, S., Isaksson, L. A., Sekine, Y., Ohtsubo, E., Zhang, S., Goon, S., Nelken, S., Shuda, M., and Kaji, A. (1998) Evidence for in vivo ribosome recycling, the fourth step in protein biosynthesis, *EMBO J. 17*, 1141−1151.
13. Janosi, L., Mori, H., Sekine, Y., Abragan, J., Janosi, R., Hirokawa, G., and Kaji, A. (2000) Mutations influencing the frr gene coding for ribosome recycling factor (RRF), *J. Mol. Biol. 295*, 815−829.
14. Karimi, R., Pavlov, M. Y., Buckingham, R. H., and Ehrenberg, M. (1999) Novel roles for classical factors at the interface between translation termination and initiation, *Mol. Cell 3*, 601−609.
15. Kiel, M. C., Raj, V. S., Kaji, H., and Kaji, A. (2003) Release of ribosome-bound ribosome recycling factor by elongation factor G, *J. Biol. Chem. 278*, 48041−48050.
16. Rao, A. R., and Varshney, U. (2001) Specific interaction between the ribosome recycling factor and the elongation factor G from *Mycobacterium tuberculosis* mediates peptidyl-tRNA release and ribosome recycling in *Escherichia coli*, *EMBO J. 20*, 2977−2986.
17. Vizcaino, N., Cloeckaert, A., Dubray, G., and Zygmunt, M. S. (1996) Cloning, nucleotide sequence, and expression of the gene coding for a ribosome releasing factor-homologous protein of *Brucella melitensis*, *Infect. Immun. 64*, 4834−4837.
18. Hirashima, A., and Kaji, A. (1972) Factor-dependent release of ribosomes from messenger RNA. Requirement for two heat-stable factors, *J. Mol. Biol. 65*, 43−58.
19. Kaji, A., Kiel, M. C., Hirokawa, G., Muto, A., Inokuchi, Y., and Kaji, H. (2001) The fourth step of protein synthesis, disassembly of the post-termination complex is catalyzed by elongation factor G and ribosome recycling factor, RRF, a near perfect mimic of tRNA, in *Cold Spring Harbor Symposia on Quantitative Biology, The Ribosome*, pp 515−529, Cold Spring Harbor Laboratory Press, Plainview, NY.
20. Rodnina, M. V., and Wintermeyer, W. (1995) GTP consumption of elongation factor Tu during translation of heteropolymeric mRNAs, *Proc. Natl. Acad. Sci. U.S.A. 92*, 1945−1949.
21. Bradford, M. M. (1976) A rapid and sensitive method for the quantitation of microgram quantities of protein utilizing the principle of protein-dye binding, *Anal. Biochem. 72*, 248−254.
22. Wilson, K. S., and Noller, H. F. (1998) Mapping the position of translational elongation factor EF-G in the ribosome by directed hydroxyl radical probing, *Cell 92*, 131−139.
23. Rohrbach, M. S., Bodley, J. W., and Mann, K. G. (1975) Chemical and physical studies on the structure of *Escherichia coli* elongation factor G, *J. Biol. Chem. 250*, 6831−6836.
24. Deng, H. Y., Odom, O. W., and Hardesty, B. (1986) Localization of L11 on the *Escherichia coli* ribosome by singlet−singlet energy transfer, *Eur. J. Biochem. 156*, 497−503.
25. Lakowicz, J. R. (1999) *Principles of fluorescence spectroscopy*, 2nd ed., Kluwer Academic/Plenum Press, New York.
26. Fersht, A. (1999) *Structure and mechanism in protein science, a guide to enzyme catalysis and protein folding*, W. H. Freeman & Company, New York.
27. Ellman, G. L. (1958) A colorimetric method for determining low concentrations of mercaptans, *Arch. Biochem. Biophys. 74*, 443−450.
28. Nakano, H., Yoshida, T., Uchiyama, S., Kawachi, M., Matsuo, H., Kato, T., Ohshima, A., Yamaichi, Y., Honda, T., Kato, H., Yamagata, Y., Ohkubo, T., and Kobayashi, Y. (2003) Structure and binding mode of a ribosome recycling factor (RRF) from mesophilic bacterium, *J. Biol. Chem. 278*, 3427−3436.

29. Baca, O. G., Rohrbach, M. S., and Bodley, J. W. (1976) Equilibrium measurements of the interactions of guanine nucleotides with *Escherichia coli* elongation factor G and the ribosome, *Biochemistry 15*, 4570−4574.
30. Rodnina, M. V., Savelsbergh, A., Matassova, N. B., Katunin, V. I., Semenkov, Y. P., and Wintermeyer, W. (1999) Thiostrepton inhibits the turnover but not the GTPase of elongation factor G on the ribosome, *Proc. Natl. Acad. Sci. U.S.A. 96*, 9586−9590.
31. Agrawal, A. K., Sharma, M. R., Kiel, M. C., Hirokawa, G., Booth, T. M., Spahn, C. M. T., Grassucci, R. A., Kaji, A., and Frank, J. (2004) Visualization of ribosome-recycling factor on the Escherichia coli 70S ribosome: functional implications. *Proc. Natl. Acad. Sci. U.S.A. 101*, 8900−8905.
32. Cameron, D. M., Thompson, J., Gregory, S. T., March, P. E., and Dahlberg, A. E. (2004) Thiostrepton-resistant mutants of *Thermus thermophilus*, *Nucleic Acids Res. 32*, 3220−3227.
33. Selmer, M., Al-Karadaghi, S., Hirokawa, G., Kaji, A., and Liljas, A. (1999) Crystal structure of *Thermotoga maritima* ribosome recycling factor, a tRNA mimic, *Science 286*, 2349−2352.
34. Aevarsson, A., Brazhnikov, E., Garber, M., Zheltonosova, J., Chirgadze, Y., al-Karadaghi, S., Svensson, L. A., and Liljas, A. (1994) Three-dimensional structure of the ribosomal translocase, elongation factor G from *Thermus thermophilus*, *EMBO J. 13*, 3669−3677.
35. Czworkowski, J., Wang, J., Steitz, T. A., and Moore, P. B. (1994) The crystal structure of elongation factor G complexed with GDP, at 2.7 Å resolution, *EMBO J. 13*, 3661−3668.
36. Gordon, J. (1970) Regulation of the in vivo synthesis of the polypeptide chain elongation factors in *Escherichia coli*, *Biochemistry 9*, 912−917.
37. Lambert, J. M., Boileau, G., Howe, J. G., and Traut, R. R. (1983) Levels of ribosomal protein S1 and elongation factor G in the growth cycle of *Escherichia coli*, *J. Bacteriol. 154*, 1323−1328.
38. Caldas, T., Laalami, S., and Richarme, G. (2000) Chaperone properties of bacterial elongation factor EF-G and initiation factor IF2, *J. Biol. Chem. 275*, 855−860.
39. Andersen, L. D., Moreno, J. M., Clark, B. F., Mortensen, K. K., and Sperling-Petersen, H. U. (1999) Immunochemical determination of cellular content of translation release factor RF4 in *Escherichia coli*, *IUBMB Life 48*, 283−286.
40. Agrawal, R. K., Heagle, A. B., Penczek, P., Grassucci, R. A., and Frank, J. (1999) EF-G-dependent GTP hydrolysis induces translocation accompanied by large conformational changes in the 70S ribosome, *Nat. Struct. Biol. 6*, 643−647.
41. Frank, J., and Agrawal, R. K. (2000) A ratchet-like inter-subunit reorganization of the ribosome during translocation, *Nature 406*, 318−322.
42. Savelsbergh, A., Katunin, V. I., Mohr, D., Peske, F., Rodnina, M. V., and Wintermeyer, W. (2003) An elongation factor G-induced ribosome rearrangement precedes tRNA-mRNA translocation, *Mol. Cell 11*, 1517−1523.
43. Bremer, H., and Dennis, P. P. (1996) Modulation of chemical composition and other parameters of the cell by growth rate, in *Escherichia coli and Salmonella* (Neidhart, F. C., Ed.) 2nd ed., Vol. 2, pp 1553−1569, ASM Press, Washington, DC.
44. Pavlov, M. Y., Freistroffer, D. V., MacDougall, J., Buckingham, R. H., and Ehrenberg, M. (1997) Fast recycling of *Escherichia coli* ribosomes requires both ribosome recycling factor (RRF) and release factor RF3, *EMBO J. 16*, 4134−4141.
45. Lancaster, L., Kiel, M. C., Kaji, A., and Noller, H. F. (2002) Orientation of ribosome recycling factor in the ribosome from directed hydroxyl radical probing, *Cell 111*, 129−140.
46. Noller, H. F., Yusupov, M. M., Yusupova, G. Z., Baucom, A., and Cate, J. H. (2002) Translocation of tRNA during protein synthesis, *FEBS Lett. 514*, 11−16.
47. Cameron, D. M., Thompson, J., March, P. E., and Dahlberg, A. E. (2002) Initiation factor IF2, thiostrepton and micrococcin prevent the binding of elongation factor G to the *Escherichia coli* ribosome, *J. Mol. Biol. 319*, 27−35.

BI048927P